Applied Catalysis B: Environmental 88 (2009) 185–193

Contents lists available at ScienceDirect

Applied Catalysis B: Environmental

journal homepage: www.elsevier.com/locate/apcatb

Preparation of carbon-supported Pt–Pd electrocatalysts with improved physical properties using electroless deposition methods

Kevin D. Beard, J.W. Van Zee, John R. Monnier *

Department of Chemical Engineering, University of South Carolina, Columbia, SC 29208, USA

ARTICLE INFO

Article history:
Received 30 July 2008
Received in revised form 20 September 2008
Accepted 24 September 2008
Available online 14 October 2008

Keywords:
Bimetallic catalysts
Electroless deposition
Oxygen reduction
Platinum
Palladium
Fuel cells

ABSTRACT

Surface modification of a carbon support preceding deposition of catalytic Pd seed nuclei has been used to prepare Pt–Pd catalysts by the electroless deposition (ED) of Pt (onto the Pd surface) from a solution containing $PtCl_6^{2-}$ and dimethylamine borane reducing agent. Functionalization of a carbon support with nitric acid to form surface carboxylic acid groups is followed by pre-treatment in a pH 14 bath to convert the acid moieties to the corresponding carboxylate ($RCOO^-$) groups. The negative surface charge results in an electrostatic attraction between the carboxylate groups and positively charged Pd^{2+} cations during wet impregnation to produce smaller catalytic Pd seed nuclei which act as deposition sites for Pt in the ED process. Analysis by TEM after Pt deposition indicated the Pt–Pd particle sizes were smaller and had a more narrow size distribution than a series of Pt–Rh/C catalysts prepared earlier in which there had been no such modification of the carbon surface [K.D. Beard, M.T. Schaal, J.W. Van Zee, J.R. Monnier, Applied Catalysis B: Environmental 72 (2007) 262]. Cyclic voltammetry experiments indicated the Pt–Pd/C catalysts have different (bi)sulfate anion adsorption properties than conventional Pt/C electrocatalysts, suggesting a possible change in the d-band electronic structure of the surface atoms. However, oxygen reduction activity of Pt–Pd/C is only comparable to that of the Pt/C catalyst. Regardless, the results have implications for using ED methods to decrease the amount of Pt used for the oxygen electrode in low temperature fuel cells.

1. Introduction

With the growing commercialization of fuel cells and subsequent attempts to make the technology economically competitive, much attention has been focused on lowering the cost of the membrane electrode assembly (MEA) and, specifically, the catalysts used for the oxygen reduction reaction (ORR). The most common electrocatalyst used in proton exchange membrane (PEM) fuel cells is Pt supported on electrically conductive porous carbon. One way to lower the cost of Pt in fuel cells is to minimize the particle sizes of the supported Pt catalyst and thereby increase the surface/volume ratio of the Pt particles (Pt dispersion) to achieve a more efficient use of Pt.

One promising preparative method that offers the potential for improved Pt dispersion is electroless deposition (ED). ED is a catalytic or auto-catalytic process whereby a chemical reducing agent reduces a metallic salt onto specific surface sites which can either be a catalytically active substrate [1] or an inert substrate seeded with a catalytically active metal [2]. This ED methodology, an alternative to electroplating of substrates, is also referred to as electroless plating [3]. While plating generally involves creating thin (on the order of several microns) homogeneous, metal layers and has many applications in various fields such as electronics, wear and corrosion-resistant materials, medical devices, and battery technology [4], we are interested in several angstroms of thickness and even monolayers of material. Thus, even though electrolessly deposited platinum has become commonplace in the plating industry for situations where conventional electrical deposition is not sufficiently uniform [5–7], selective and controlled deposition, as opposed to continuous plating, has just recently been examined [8–10] for applications in catalysis.

The overall reaction for ED is a combination of anodic and cathodic electrochemical partial reactions [4,5]. Reaction (1) is the overall reaction, while (2) and (3) are the anodic and cathodic partial reactions, respectively

$$N + M^{z+}(aq) + RA(aq) \rightarrow M{-}N + Ox(aq) \quad (1)$$

$$RA(aq) \rightarrow Ox(aq) + ze^- \quad (2)$$

$$N + M^{z+}(aq) + ze^- \rightarrow M{-}N \quad (3)$$

in the above reactions, Ox is the oxidation product of the reducing agent (RA) and M is the metallic form of the reducible metal salt

* Corresponding author. Tel.: +1 803 777 6813; fax: +1 803 777 8142.
E-mail addresses: beardk@engr.sc.edu (K.D. Beard), vanzee@engr.sc.edu (J.W. Van Zee), monnier@engr.sc.edu (J.R. Monnier).

0926-3373/$ – see front matter © 2008 Elsevier B.V. All rights reserved.
doi:10.1016/j.apcatb.2008.09.033

(M^{z+}) that has been deposited on the catalytic nuclei (N) which has already been deposited on the carbon support. From an electrochemical standpoint, the equilibrium potential of reaction (2) must be more negative than the equilibrium potential of reaction (3). According to the mixed potential theory, the overall system reaches an equilibrium mixed potential E_{mp} during steady state which is found by equating the currents of the two partial reactions. A further corollary of the above equations is that the site for oxidation of the reducing agent is in close spatial proximity to the site for the reduction of the cation of the metal salt; therefore, the metal cation is reduced and deposited on the same surface near the activated reducing agent. Our earlier work showed that deposition of Pt on the carbon support alone could be completely inhibited under the correct ED conditions. In addition, because the deposited metal in reaction (3) is typically catalytic for reaction (3), further reduction can occur (auto-catalysis), potentially resulting in formation of multiple layers, or a shell, of M, if reaction conditions permit according to reaction (4):

$$M + M^{z+}(aq) + RA(aq) \rightarrow M{-}M + Ox(aq) \quad (4)$$

This communication extends our earlier work on the methodology of ED for the preparation of next generation PEMFC electrocatalysts [11]. As shown below we increase Pt dispersion in ED-derived catalysts through a procedure to provide a more highly dispersed Pd precursor compared to the Rh precursor previously used. Since the platinum is deposited only on the surface of either the Pd precursor or the just-deposited Pt, smaller precursor particles should present a greater surface concentration of catalytic sites for Pt deposition to give smaller, final Pt–Pd particles with higher Pt dispersions. Therefore, a primary objective of this second generation of ED catalysts is to identify precursor compounds that formed smaller, catalytic seed particles compared to those using $Rh_4(CO)_{12}$ as a precursor [11].

To achieve greater Pd precursor dispersion, an interaction between support and precursor compound is critical. According to Sepulveda-Escribano et al. [12], the strength of precursor–support interactions results from factors such as polarity of the solvent, pH of the impregnating solution, cationic/anionic nature of the precursor, and the isoelectric point of the support (or point of zero charge, PZC). For carbon supports this interaction has been obtained by pretreatment with an oxidizing agent such as nitric acid [13–21], hydrogen peroxide [12,14,17,18,22], and high temperature oxygen [15,16] to introduce oxygen-containing functional groups such as carboxylic acid groups. These oxygen-containing functional groups affect the carbon surface by (1) providing nucleation sites for deposition of precursor compounds [15,16], (2) forming "anchor" sites to lower the extent of metal agglomeration [13,17,20], (3) increasing the hydrophilicity of the surface [15,16], and (4) changing the intrinsic PZC of the support [17,23–26]. Specifically, the adsorption of noble metal salts onto many supports, including carbon, is initiated as a coulombic process. Thus, if the pH of the impregnation solution is below the PZC of the support, surface oxygen functionalities such as bridging or terminal oxygen and carboxylate groups will be protonated and interact more strongly with negatively charged salts; conversely, if the pH is higher than the PZC, positively charged salts interact more strongly with the support.

2. Experimental

2.1. Catalyst synthesis

Using the general procedure discussed in previous work [11], Vulcan XC-72 (254 m^2/g), from Cabot Corporation, [27] was wet-impregnated with different Pd compounds to activate the subsequent ED of platinum. Prior to Pd salt impregnation, the XC-72 carbon was cleaned and oxidized in 5 M HNO_3 for 2 h at 50 °C and then rinsed with de-ionized water and dried under vacuum. This oxidative treatment should populate the carbon surface with carboxylic acid groups. Next, the carbon was pretreated at 50 °C in a pH 14 bath for 60 min to convert the surface carboxylic acid groups to the corresponding carboxylate ($RCOO^-$) groups. The negative charge should result in an electrostatic attraction between the carboxylate groups and positively charged Pd^{2+} cations during wet impregnation. Three different Pd precursors were examined: an organometallic compound [bis-allyl palladium chloride, $(C_3H_5)_2PdCl_2$], a salt of an organic acid [palladium acetate, $Pd(C_2H_3O_2)_2$], and an ionic salt [tetraamine palladium nitrate, $(NH_3)_4Pd(NO_3)_2$], all supplied by Strem Chemicals. Dichloromethane (Acros Organics) was used as the solvent for the bis-allyl palladium chloride and the palladium acetate, while methanol (JT Baker) and de-ionized water were used as solvents for the tetraamine palladium nitrate.

Following wet impregnation of the Pd salts, excess solvent was removed by rotary evaporation at 30 °C (CH_2Cl_2), 60 °C (CH_3OH), and 80 °C (de-ionized H_2O) under vacuum. Reduction of the Pd precursor compound to metallic palladium was obtained by exposure of the impregnated carbon support to an aqueous solution of sodium borohydride (molar ratio of BH_4^-/Pd^{2+} = 10) at room temperature.

Platinum was then deposited on the palladium by ED using a bath containing H_2PtCl_6, dimethylamine borane (DMAB) and sodium citrate. The conditions used for all ED baths were 1:5:5 molar ratio of Pt to DMAB to citrate at an initial pH of 11. Deposition times were kept constant at 30 min and the temperature was maintained at 80 °C. For all samples the maximum theoretical platinum loading was maintained at 8.4% by weight, based on the amount of H_2PtCl_6 in the ED bath. Preliminary work indicated that deposition of Pt was essentially complete after 30 min.

2.2. Characterization methods

The percent weight loadings of Pt and Pd (defined as $100 \times g_{metal}/g_{catalyst}$) were determined by atomic absorption (Perkin-Elmer 3300 Spectrometer) using conventional analysis protocols. Palladium dispersions and average palladium particle diameters were determined by H chemisorption (Quantachrome Gas Sorption System); CO was used to validate the hydrogen data; no indication of β-PdH formation was observed in any of the H chemisorption analyses. Transmission electron microscopy (TEM) (Hitachi H-8000) was used to determine the average particle sizes and particle size distributions for the Pt–Pd catalysts after Pt was electrolessly deposited on the different Pd/C precursor catalysts. The micrograph images were measured manually to calculate average Pt particle sizes. In all cases, a statistically relevant number of Pt particles were measured to ensure valid size distributions. For comparison, a 20-wt% Pt/XC-72 commercial catalyst from E-Tek was also analyzed by TEM. Since the palladium particles were too small (<1.0–1.5 nm) for the resolution of the TEM, it was not possible to measure the Pd/C precursor catalysts synthesized by wet impregnation.

Electrochemical characterization was conducted using a glassy-carbon rotating disk electrode (RDE) with a surface area of 0.287 cm^2 attached to a Pine Instruments AFASR rotator and a Princeton Applied Research PAR-273A or PAR-283 Potentiostat. Catalyst films were prepared on the RDE from sonicated aliquots of a catalyst suspension containing 2.8 $mg_{catalyst}$/mL to give a Pt mass of 5.6 μg per film. The catalyst films were fixed to the RDE with a 5-μL aliquot

of a 20:1 isopropyl alcohol:Nafion® solution and subsequent evaporation of the alcohol at room temperature. Three replicates of the films were used to obtain the kinetic data. A standard calomel electrode, isolated from the system by a Luggin capillary, was used as the reference electrode and voltages were converted and are reported relative to the standard hydrogen electrode (SHE). The counter electrode was a Pt wire and was also isolated by enclosure in a glass tube with a fritted ending. Electroactive surface area measurements were conducted in a de-aerated 0.1 M $HClO_4$ or 0.5 M H_2SO_4 electrolyte at 5 mV/s, 10 mV/s, and 25 mV/s scan rates. The ORR kinetic analysis was performed in 0.1 M $HClO_4$ or 0.5 M H_2SO_4 electrolyte solutions saturated with O_2 at a scan rate of 1 mV/s and rotation rates between 250 rpm and 2400 rpm. All electrochemical tests were conducted at room temperature.

3. Results and discussion

3.1. Effect of carbon pretreatment

Three Pd precursor compounds were examined to determine if smaller Pd particles could be prepared relative to the $Rh_4(CO)_{12}$ precursor used in earlier work [11]. To further enhance precursor dispersion, the carbon support was oxidized in HNO_3 and then pretreated with a pH 14 bath (as described above) prior to wet impregnation of the Pd compounds. An electrostatic attraction should result in stronger interactions between the carbon surface and the Pd salts during impregnation as shown in Table 1 where the pH 14 treatment is contrasted to no pretreatment. The pH 14 pretreatment resulted in a decrease of Pd particle size for both the $(C_3H_5)_2PdCl_2$ and $Pd(C_2H_3O_2)_2$ precursors; however, the effect is more pronounced with the $Pd(C_2H_3O_2)_2$, most likely because the $(C_3H_5)_2PdCl_2$ dimer is an organometallic compound, not a salt, and should not dissociate as extensively as $Pd(C_2H_3O_2)_2$. Based on the results of the pH 14 pretreatment, all subsequent catalysts were prepared using a support pretreated in an aqueous bath at pH 14 at 50 °C for 60 min, followed by washing with de-ionized H_2O. After drying at 100 °C in vacuo, the support was ready for impregnation by the different Pd compounds.

3.2. Evaluation of Pd precursor catalysts

Carbon-supported Pd catalysts made from the precursors $(C_3H_5)_2PdCl_2$, $Pd(C_2H_3O_2)_2$, and $(NH_3)_4Pd(NO_3)_2$ were examined using H_2 chemisorption to determine average Pd particle sizes and dispersions. The chemisorption data, summarized in Table 2, show that at 0.5% Pd loading, the $(C_3H_5)_2PdCl_2$ precursor forms larger Pd particle sizes than the other combinations of Pd precursor compounds and solvents. Therefore, no additional Pd precursor catalysts were synthesized using $(C_3H_5)_2PdCl_2$.

The data in Table 2 for $Pd(C_2H_3O_2)_2$ also show that Pd particle sizes remain approximately constant as the Pd weight loading increases from 0.5% to 5.0%, indicating that formation of additional similarly sized particles rather than formation of larger Pd particles is favored. Thus, the number of Pd seed particles increases with Pd loading, which should result in the formation of more Pt–Pd particles during the deposition of Pt. In contrast, the $(NH_3)_4Pd(NO_3)_2$/de-ionized H_2O combination increases Pd particle sizes as Pd loading increases from 0.5% to 2.5%, indicating that Pd particle growth is favored over nucleation. This result is consistent with the hydrophobic nature of most carbon surfaces [15,16]. The inability of water to wet the carbon surface results in "puddling" of Pd salts on the carbon surface, a phenomenon leading to Pd particle growth as the water is removed during drying. When CH_3OH, rather than de-ionized H_2O, is used as the solvent for $(NH_3)_4Pd(NO_3)_2$, the results are much different. There are only small changes in average Pd particle diameters as the Pd weight loading increases from 0.5% to 2.5%, suggesting again that more Pd particles of the same diameter are being deposited instead of growth of larger Pd particles. This is also consistent with the observation that organic solvents (such as methanol) wet carbon surfaces more efficiently than water.

Table 1
Effect of carbon support pretreatment. Average Pd particle diameters were determined by H chemisorption. Dispersion values were calculated from chemisorption data.

Pd loading (%)	Precursor compound	Pre-treatment	Average Pd particle diameter (Å)	Pd dispersion (%)
0.5	$(C_3H_5)_2PdCl_2$	None	72	15.5
0.5	$(C_3H_5)_2PdCl_2$	pH 14 bath	57	19.7
0.5	$Pd(C_2H_3O_2)_2$	None	117	9.5
0.5	$Pd(C_2H_3O_2)_2$	pH 14 bath	33	34.5

Table 2
Results of H_2 chemisorption analysis for Pd precursor catalysts. Pd dispersion was calculated from chemisorption data. Average Pd diameters were then calculated from dispersion values.

Precursor compound	Solvent	Pd loading (%)	Average Pd particle diameter (Å)	Pd dispersion (%)
$(C_3H_5)_2PdCl_2$	CH_2Cl_2	0.5	57	19.7
$Pd(C_2H_3O_2)_2$	CH_2Cl_2	0.5	33	34.5
		1.0	41	27.6
		2.5	38	29.8
		5.0	40	28.3
$(NH_3)_4Pd(NO_3)_2$	H_2O	0.5	33	34.5
		1.0	66	17.2
		2.5	85	13.3
$(NH_3)_4Pd(NO_3)_2$	CH_3OH	0.5	40	28.3
		1.0	33	34.5
		2.5	40	38.3

3.3. TEM characterization

The TEM results are summarized in Table 3 and sample images are shown in Figs. 1–3. Also included in Table 3 for comparison are data for Pt deposited on the Rh/C samples which were discussed in our previous work [11]. Analysis of TEM images permits the direct determination of average Pt–Pd particle diameters. To calculate the total concentration of surface Pt and Pd sites per gram of catalyst and the concentration of Pt–Pd particles per gram of catalyst, a weighted unit cell parameter based on the mole ratio of Pt and Pd must be used. This is justified because both Pt and Pd exist in face-centered cubic (fcc) lattices with almost identical unit cell parameters of 3.92 Å and 3.89 Å, respectively. Since the mono-metallic structures of the two metals are quite similar (<1% difference in unit cell parameters), we can calculate a weighted average unit cell parameter based on molar loadings of Pt and Pd in that particular composition. This weighted unit cell parameter is used to determine the sum of surface Pt and Pd sites per gram of catalyst and the concentration of Pt–Pd particles per gram of catalyst. These data are summarized in Table 3. Additionally, the atomic ratios of Pt:Pd for the samples prepared by $Pd(C_2H_3O_2)_2$ are 7.6, 4.6, 1.8, and 0.9 for Pd weight loadings of 0.5%, 1.0%, 2.5%, and 5.0%, respectively. The analogous atomic ratios for the Pt–Rh/C samples were 7.3, 1.6, and 0.8 for Rh weight loadings of 0.4%, 2.2%, and 4.4%, respectively.

The particle sizes in Table 3 calculated from TEM images are not consistent with the average Pd particle diameters in Table 2 that

Table 3
Results of TEM analysis. Concentration of surface sites is given as the sum of both Pd and Pt atoms, since it was not possible to determine the exact composition of the surface. ED kinetics indicates that both catalytic and autocatalytic deposition may occur, resulting in a surface containing both Pd and Pt atoms. The $Rh_4(CO)_{12}$ data are from Ref. [11].

Precursor compound	Precursor loading (Pd or Rh) (%)	Pt loading (%)	TEM characterization		
			Avg. Pt–Pd particle diameter (Å)	Concentration of surface Pt–Pd sites/$g_{catalyst}$	Concentration of Pt–Pd particles/$g_{catalyst}$
$Pd(C_2H_3O_2)_2$	0.5	7.0	35	7.8×10^{19}	2.0×10^{17}
	1.0	8.4	32	1.1×10^{20}	4.0×10^{17}
	2.5	8.4	30	1.5×10^{20}	6.5×10^{17}
	5.0	8.4	32	1.9×10^{20}	8.4×10^{17}
$(NH_3)_4Pd(NO_3)_2/H_2O$	0.5	7.6	40	7.5×10^{19}	1.8×10^{17}
	1.0	8.0	34	1.0×10^{20}	3.4×10^{17}
	2.5	8.5	34	1.3×10^{20}	5.3×10^{17}
$(NH_3)_4Pd(NO_3)_2/CH_3OH$	0.5	7.6	35	8.4×10^{19}	2.4×10^{17}
	1.0	8.2	34	1.0×10^{20}	3.5×10^{17}
	2.5	8.1	28	1.6×10^{20}	7.6×10^{17}
E-Tek 20% Pt/C	n/a	19.2	40	1.7×10^{20}	4.4×10^{17}
$Rh_4(CO)_{12}$	0.4	5.5	69	2.8×10^{19}	1.7×10^{16}
	2.2	6.8	51	4.6×10^{19}	5.4×10^{16}
	4.4	6.8	32	7.5×10^{19}	2.4×10^{17}

were calculated from H chemisorption data. That is, Table 2 shows that the Pd particles which acted as catalytic nuclei for Pt deposition are larger than the Pt–Pd particles; this is not physically possible because the addition of Pt to Pd can only increase the final particle size. One explanation for this disparity is that the sizes in Table 2 are a result of agglomeration due to the pretreatment before chemisorption. The pretreatment requires that samples are reduced at 200 °C in flowing H_2 for 2 h and then evacuated for two additional hours at the same temperature before cooling to 35 °C for the chemisorption analysis. The high temperature treatment

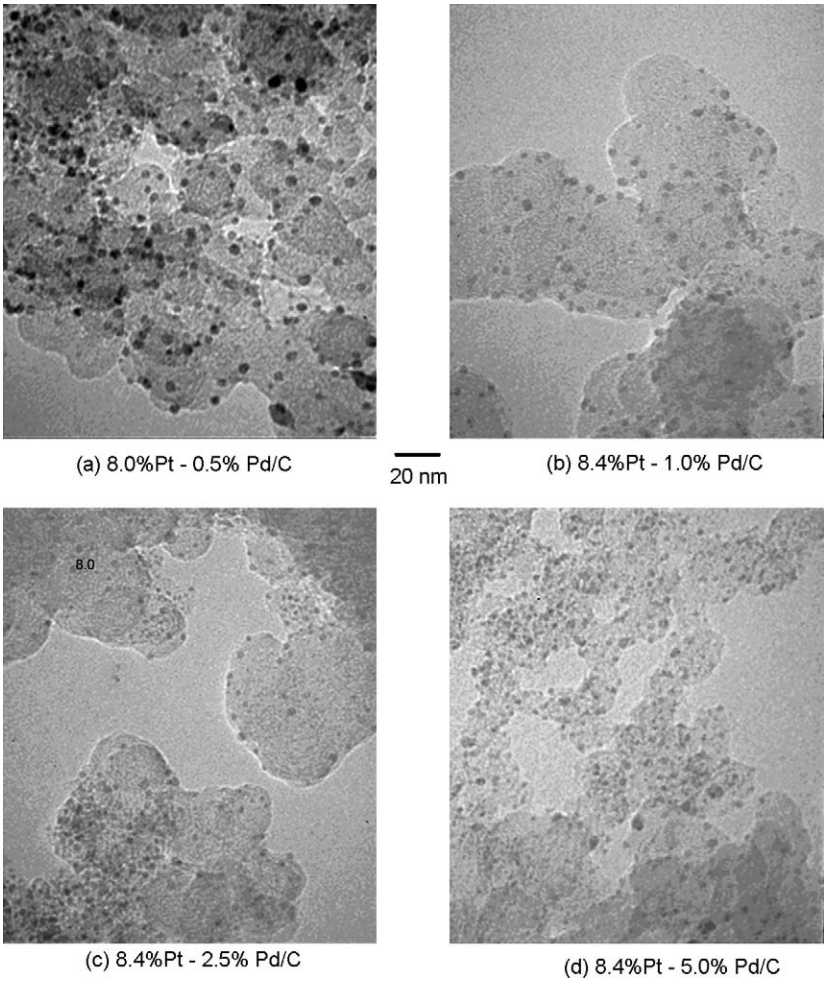

Fig. 1. TEM images for Pt electrolessly deposited on Pd/C using $Pd(C_2H_3O_2)_2$ in CH_2Cl_2 solvent as the Pd precursor. Scale in the middle is applicable to all images.

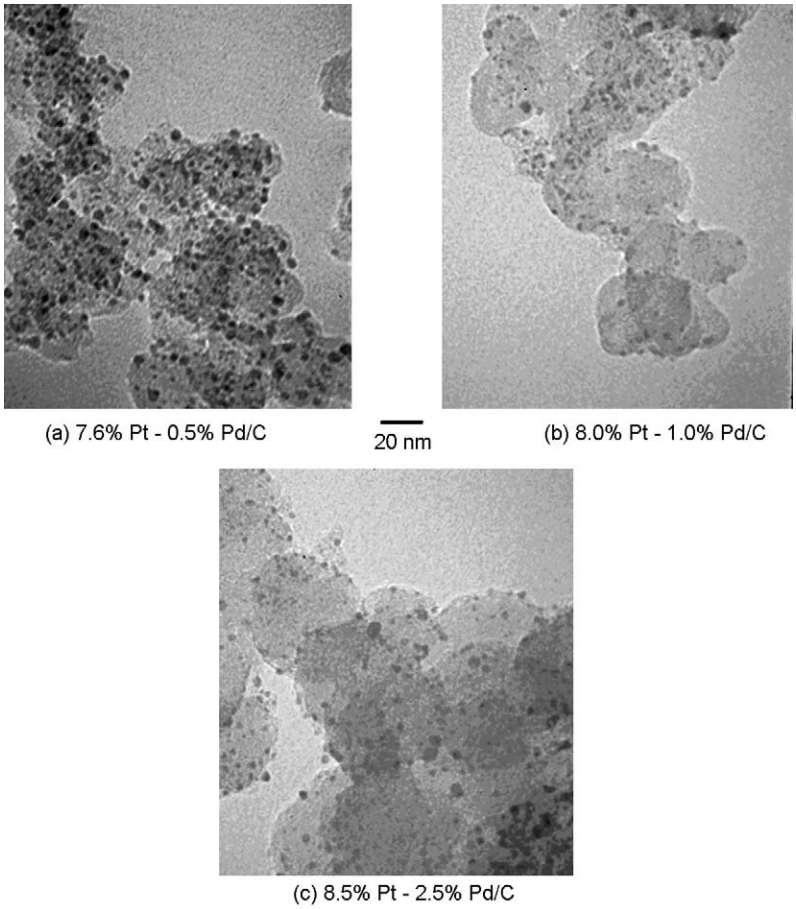

Fig. 2. TEM images for Pt electrolessly deposited on Pd/C using $(NH_3)_4Pd(NO_3)_2$ in de-ionized H_2O solvent as the Pd precursor. Scale in the middle is applicable to all images.

prior to chemisorption is essential to ensure reduction of the Pd particles, to remove all water in the sample, and to attain the high vacuum conditions required for chemisorption; however, it may also cause agglomeration of Pd particles. Gurrath et al. [28] observed that palladium particles supported on carbon began to agglomerate at temperatures as low as 100 °C, while Suh et al. [29] and Heal and Mkayula [30] both reported agglomeration of palladium particles supported on carbon subjected to temperatures of 200 °C or less over a one hour time period. Another possible explanation is that it may not be possible to directly compare particle sizes measured by TEM with those calculated from chemisorption methods. The TEM method examines only a small part of the overall surface while chemisorption gives an average particle size determined by total uptake of selective adsorbate (H_2, in this case) for the whole sample. Independent of the reason for this discrepancy, the data in Table 2 can be used for determining the proper combination of Pd precursor and solvent for the subsequent ED experiments and chemisorption was not used to examine the Pt–Pd catalysts prepared by ED. Note that the highest temperature used during ED was 80 °C.

As shown in Table 3, the final particle diameters decrease with increasing Pd loading for samples prepared by ED. This is because Pd particle nucleation is favored over Pd particle growth as the Pd loading increases, which results in the formation of more Pd seed sites for ED of Pt. The concentrations of Pd particles for the different precursor compositions are shown in the last column of Table 3. These concentrations are actually calculated from the number and distribution of the Pt–Pd bimetallic particles that were determined by TEM. Since Pt-containing particles are only formed on Pd precursor particles, the number of Pd precursor particles is equal to the number of Pt–Pd particles measured by TEM. Thus, when similar loadings of Pt are electrolessly deposited on a greater number of Pd seed particles, the final Pt–Pd particle sizes decrease. One exception in Table 3 is the Pt–Pd average particle diameter for 5.0% Pd loading (prepared from $Pd(C_2H_3O_2)_2$) which increases compared to that for 2.5% Pd loading, suggesting that increasing Pd loading from 2.5% to 5.0% favors both particle growth and nucleation. Table 3 also shows that the Pt–Pd particles have a smaller average diameter than comparable Pt–Rh particles. Direct comparisons between Rh particle sizes as measured by TEM [11] and Pd particle sizes as measured by H chemisorption are not possible for reasons outlined above; however, an indirect comparison can be made between Pt–Pd and Pt–Rh particle sizes as measured by TEM. Since both the amounts of Pt deposited on the Pd/C are greater than that deposited on the Rh/C and the final Pt–Pd particle diameters are lesser than that for Pt–Rh, the average Rh particle size must be much larger than the Pd particle size.

In addition to calculation of average particle diameters of the Pt–Pd particles, analysis of the TEM images permits the determination of particle size distribution curves which are shown in Figs. 4–6 for the samples prepared using $Pd(C_2H_3O_2)_2$, $(NH_3)_4Pd(NO_3)_2/CH_3OH$, and $(NH_3)_4Pd(NO_3)_2/H_2O$, respectively, as Pd precursors. Also included for comparison purposes are the results for Pt deposited on the $Rh_4(CO)_{12}$ precursor [11] and the 20% Pt/C catalyst (E-Tek). Since both Pd (106.4 g/mole) and Rh (102.9 g/mole) have similar atomic weights, similar weight loadings correspond to comparable molar loadings of each component.

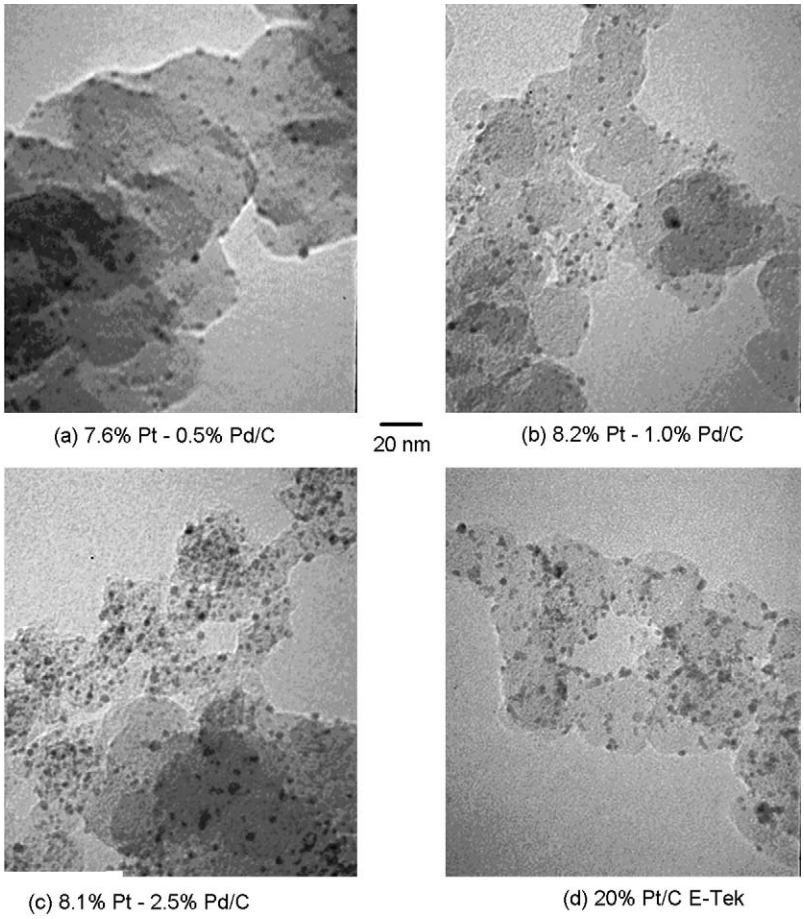

Fig. 3. TEM images for Pt electrolessly deposited on Pd/C using $(NH_3)_4Pd(NO_3)_2$ in CH_3OH solvent as the Pd precursor. TEM image for the standard 20% Pt/C (E-Tek) sample is also shown. Scale in the middle is applicable to all images.

The total number of Pt–Pd particles measured for each sample in the distribution curves was approximately 500 ± 50 to provide a statistically relevant number of particles. In all cases, samples prepared using Pd/C precursors demonstrated a shift in particle size distribution toward smaller average particle sizes compared to both the $Rh_4(CO)_{12}$ precursor and the E-Tek Pt/C catalyst. In addition, the particle size distribution curves in Figs. 4–6 indicate the Pt–Pd particle size distributions are considerably narrower than for both the Pt–Rh and the commercial 20% Pt/C sample. This narrower particle size distribution also increases the Pt–Pd dispersion because the volume of a particle increases with the cube of the diameter. Thus, larger particles consume greater amounts of platinum that are contained within the bulk of the larger Pt–Pd particles, making them unavailable at the surface for electrocatalysis.

3.4. Electrochemical characterization

The Pt–Pd catalyst with the best particle size characteristics (8.4% Pt–2.5% Pd/C, $Pd(C_2H_3O_2)_2$ precursor, CH_2Cl_2 solvent) was characterized electrochemically and compared to the E-Tek

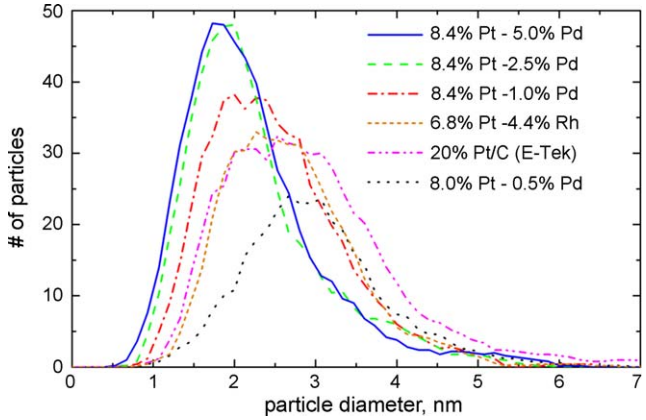

Fig. 4. Pt–Pd particle diameter distribution for ED catalysts. Pd/C was prepared from $Pd(C_2H_3O_2)_2$ in CH_2Cl_2 solvent. Analogous data for Pt–Rh from $Rh_4(CO)_{12}$ precursors [11] and 20% Pt/C E-Tek catalyst are included for comparison.

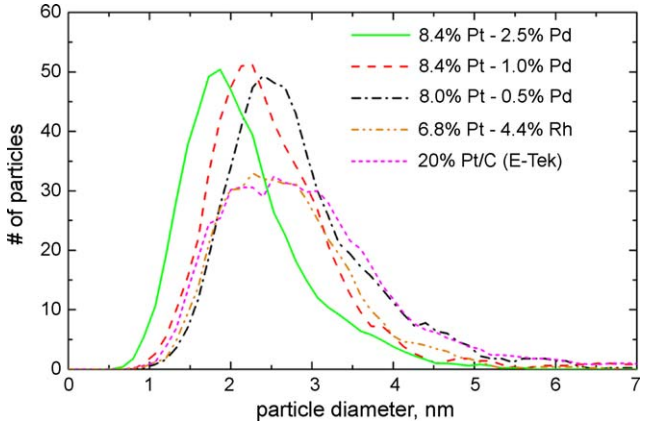

Fig. 5. Particle diameter distribution for Pt–Pd catalysts. Pd was prepared from $(NH_3)_4Pd(NO_3)_2$ in CH_3OH solvent. Analogous data for Pt–Rh from $Rh_4(CO)_{12}$ precursors [11] and 20% Pt/C E-Tek catalyst are included for comparison.

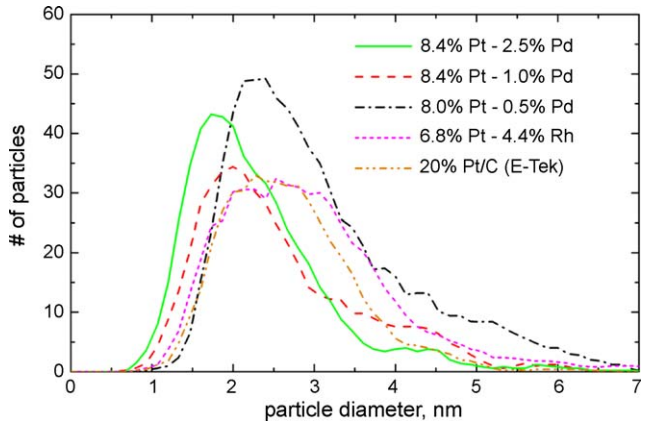

Fig. 6. Particle diameter distribution for Pt–Pd catalysts. Pd prepared from $(NH_3)_4Pd(NO_3)_2$ in de-ionized H_2O solvent. Analogous data for Pt–Rh from $Rh_4(CO)_{12}$ precursors [11] and 20% Pt/C E-Tek catalyst are included for comparison.

catalyst using a rotating disk electrode (RDE) to determine the active electrochemical surface area (ESA) and the kinetics of the ORR. For the ESA, cyclic voltammetry (CV) was performed in a de-aerated electrolyte solution while the latter was tested in an O_2-saturated electrolyte. To determine the ESA, the area under the hydrogen desorption peaks was measured between 0.05 V and 0.25 V and converted to surface area using the constant 210 μC/cm^2 [31]. The hydrogen adsorption peak (i.e., 0.05 V and 0.25 V) was less reproducible than the hydrogen desorption peak and had an unusually high apparent surface area which might indicate the occurrence of a Faradaic reaction. Each film was tested at three different sweep rates; the areas under the hydrogen adsorption/desorption peaks were approximately the same after double-layer capacitance was removed. Fig. 7 shows cyclic voltammograms of the ED catalyst and the 20% Pt/C E-Tek standard catalyst in two different electrolyte solutions (H_2SO_4 and $HClO_4$). For each sample,

Table 4
ESA results from hydrogen desorption peak analysis.

Electrolyte	Pt loading (%)	Pd loading (%)	Catalyst mass (μg)	Pt mass (μg)	Desorption area (cm^2)
$HClO_4$	20 (E-Tek)	n/a	28	5.6	4.5 ± 0.3
$HClO_4$	8.4	2.5	70	5.6	6.0 ± 0.1
H_2SO_4	20 (E-Tek)	n/a	28	5.6	14.6 ± 0.5
H_2SO_4	8.4	2.5	70	5.6	9.5 ± 0.8

the total mass of Pt is constant at 5.6 μg of Pt corresponding to 71 μg of ED catalyst and 28 μg of 20% Pt/C.

For both electrolytes, the E-Tek catalyst demonstrated dual hydrogen desorption peaks around 0.1 V, indicative of H_2 desorption from two different Pt surface orientations while the ED catalyst had only a single, broad desorption peak, suggesting a more uniform surface Pt orientation, a more complex desorption peak from both Pt and Pd sites, or a bimetallic Pt–Pd surface. In addition, the electrochemically active surface area was dependent on the choice of electrolyte. For the H_2SO_4 electrolyte, the E-Tek catalyst had a greater surface area than the Pt–Pd catalyst; however, in $HClO_4$, the results were reversed with the Pt–Pd catalyst possessing roughly 35% more surface area per gram of Pt. These results are shown in Table 4. Since the surface area changes with electrolyte, the difference likely results from preferential adsorption of the electrolyte anions ((bi)sulfate for sulfuric acid and perchlorate for perchloric acid). Perchlorate is considered to be a non-adsorbing electrolyte, thus the (bi)sulfate anion is most likely responsible for the differences in surface area. Specifically, electronic interaction between Pt and Pd results in a stronger adsorption between the Pt–Pd surface and the (bi)sulfate anion compared to unmodified Pt. This type of bimetallic interaction has been reported by others [32–34], although it is unclear whether this is the result of lattice strain between layers of Pt and Pd or electronic ligand effects, both of which would affect the d-band center with respect to the Fermi level.

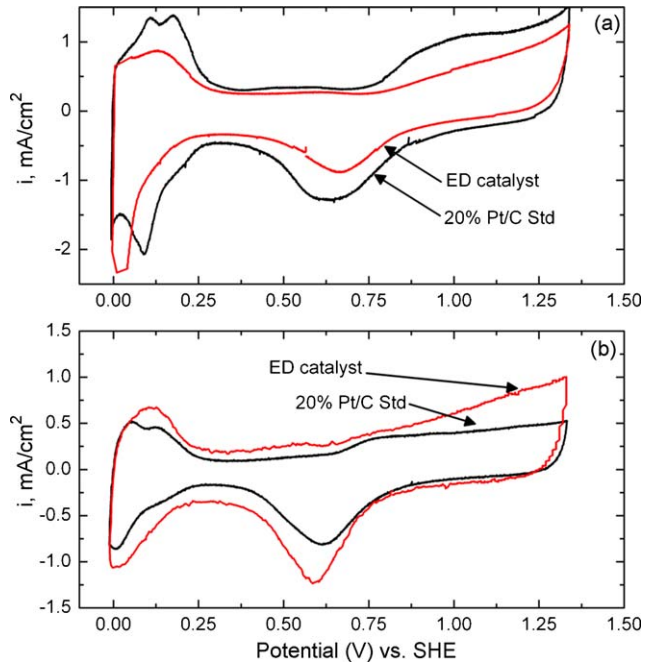

Fig. 7. Typical CV's for 71 μg of 8.4% Pt–2.5% Pd/C [$Pd(C_2H_3O_2)_2$] and 28 μg of 20% Pt/C E-Tek catalyst in 0.5 M H_2SO_4 (a) and 0.1 M $HClO_4$ (b). The scan rate = 25 mV/s and the total Pt mass = 5.6 μg.

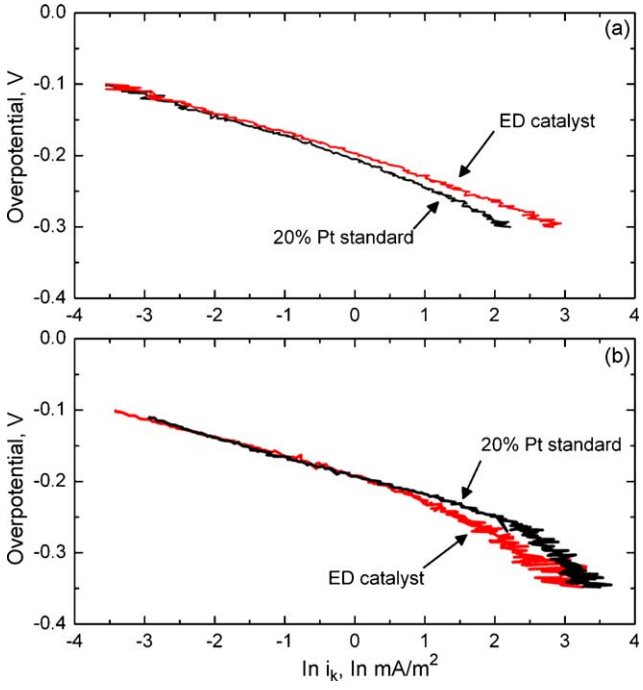

Fig. 8. Tafel region for 8.4% Pt–2.5% Pd/C (ED-derived catalyst) and 20% Pt/C (E-Tek), each with 5.6 μg Pt. All data were taken at 500 rpm rotation speed and 1 mV/s scan rate in (a) 0.1 M $HClO_4$ or (b) 0.5 M H_2SO_4 electrolyte.

Table 5
Kinetic parameters from Tafel region for oxygen reduction.

Electrolyte	Pt loading (%)	Catalyst mass (μg)	Pt mass (μg)	Tafel slope (mV/dec)	i_0 (A/cm^2)	α_c
$HClO_4$	20 (E-Tek)	28	5.6	-67.2 ± 1.5	$1.5 \pm 0.6 \times 10^{-6}$	0.22
$HClO_4$	8.4	70	5.6	-70.7 ± 3.8	$1.5 \pm 0.6 \times 10^{-6}$	0.21
H_2SO_4	20 (E-Tek)	28	5.6	-69.0 ± 6.7	$1.1 \pm 0.5 \times 10^{-6}$	0.21
H_2SO_4	8.4	70	5.6	-66.0 ± 5.5	$1.8 \pm 1.4 \times 10^{-6}$	0.22

To evaluate the ORR activity, the electrolyte was saturated with O_2 and polarization curves were measured at different rotation speeds. Both electrolytes were used in these experiments. Tafel regions in the polarization curves were identified and analyzed to determine the Tafel slope, the exchange current density, and the cathodic transfer coefficient. The Tafel regions for the two catalysts in the two different electrolytes are shown in Fig. 8 while Table 5 shows the kinetic constants determined by analysis of the Tafel region. The Tafel region was identified by the linear section from a plot of overpotential vs. ln i_k which is approximately between 0.39 V and 0.59 V vs. SHE. Mass transfer effects occur at approximately −0.3 V (overpotential) for the $HClO_4$ electrolyte and −0.25 V (overpotential) for the H_2SO_4 electrolyte [35]. The effects of mass transfer are observed in Fig. 8b for the 20% Pt/C standard sample at high currents where there is a distinct change in slope; however, kinetic constants were only taken from the most linear part of the Tafel region (approximately −0.1 V to −0.2 V of overpotential). The overpotentials were calculated by subtracting the open circuit voltage of the cathode relative to the reference electrode at the beginning of each experiment, from the voltage at a particular current during the experiment measured relative to the reference electrode. The calculations to determine kinetic constants can be found in Ref. [35].

Table 5 and Fig. 8 show that the ED catalyst has activity similar to the commercial catalyst for the ORR, even though there is some variation in the exchange current density (i_0) in H_2SO_4 due to the replicate films. This suggests that there is little interaction between the Pt and Pd components in the ED catalysts. Thus, the Pt–Pd catalyst prepared by ED does not produce a bimetallic particle that gives an electronic enhancement as predicted from computational studies [36]. There are two possible explanations for this lack of increased activity. Firstly, if the particles exist as core–shell structures, the Pt shell may be so thick that the surface Pt atoms are not affected by the presence of the Pd atoms in the Pd core. We calculate this thickness to be 3.2 monolayers of Pt shell on the Pd core if such a structure exists for the 8.4% Pt–2.5% Pd/C sample used here. Secondly, if the Pt–Pd exists as a random mixture rather than a shell–core, the structure of this mixture may be such that there is insufficient electronic interaction between Pt and Pd to produce improved ORR activity. A detailed analysis of the structure of the Pt–Pd particles is currently being conducted using XPS, which will be the subject of a forthcoming article [37].

4. Conclusion

Pt–Pd bimetallic catalysts have been prepared by surface modification of a carbon support before impregnation of Pd compounds that were subsequently reduced to form Pd seed nuclei for electroless deposition of Pt onto the Pd surfaces. The carbon surface was functionalized by treating in 5 M nitric acid for 2 h at 50 °C to form carboxylic acid sites which were then deprotonated by immersing into a pH 14 bath for 1 h at 50 °C to convert the acid moieties to carboxylate ($RCOO^-$) groups. The negative surface charge created an electrostatic attraction with positive Pd^{2+} cations during wet impregnation to form smaller Pd seed particles after BH_4^- reduction. Comparison of Pd dispersions measured by chemisorption with and without the pH 14 treatment indicated that deprotonation had a positive effect on decreasing Pd particle sizes when the Pd precursor compound was an ionic salt.

Three different Pd precursor compounds [$(C_3H_5)_2PdCl_2$, $Pd(C_2H_3O_2)_2$, $(NH_3)_4Pd(NO_3)_2$] and solvents (CH_2Cl_2, de-ionized H_2O, and CH_3OH) were used to synthesize Pd/C precursor catalysts by wet impregnation. H_2 chemisorption results indicated that the $Pd(C_2H_3O_2)_2/CH_2Cl_2$ and $(NH_3)_4Pd(NO_3)_2/CH_3OH$ impregnation systems produced the smallest Pd particle diameters (3.0–4.0 nm) and that particle sizes were independent of Pd loadings over a range from 0.5 Pd wt% to 5.0 Pd wt%. Conversely, the $(NH_3)_4Pd(NO_3)_2$/de-ionized H_2O system produced larger Pd particles ranging in size from 3.3 nm to 8.5 nm as the Pd loadings increased from 0.5 wt% to 2.5 wt% which is consistent with the "puddling" effect of H_2O on hydrophobic carbon surfaces. Impregnation of $(C_3H_5)_2PdCl_2$, an organometallic dimer, resulted in large Pd particles (5.7 nm) at a 0.5-wt% Pd loading because of the low extent of dissociation into ionic components compared to $Pd(C_2H_3O_2)_2$ and $(NH_3)_4Pd(NO_3)_2$.

Analysis by TEM after Pt deposition showed that the Pt–Pd particle sizes were smaller and had a more narrow size distribution than both the Pt–Rh particles synthesized in previous work [11] and the Pt particles in a 20% Pt/C E-Tek standard catalyst. The concentration of Pt–Pd particles was greater than that of the Pt particles in the E-Tek catalyst, 8.4×10^{17} particles/g catalyst and 4.4×10^{17} particles/g catalyst, respectively. Increasing the Pd weight loadings from 0.5% to 5.0% for $Pd(C_2H_3O_2)_2$ and from 0.5% to 2.5% for $(NH_3)_4Pd(NO_3)_2$ (CH_3OH solvent) decreased the final Pt–Pd particle sizes after deposition of Pt, indicating that the formation of more Pd nucleation sites is favored over Pd particle growth for these Pd loadings.

The electrochemical behavior (using an RDE assembly) of the best Pt–Pd catalyst, 8.4% Pt–2.5% Pd/C, was compared with that for the commercially available E-Tek catalyst at identical Pt masses. Cyclic voltammetry results showed a difference in adsorptive properties of (bi)sulfate between the two catalysts, suggesting a possible change in the d-band electronic structure for the surface of the Pt–Pd/C. However, analysis of the Tafel regions from the polarization curves taken in aerated electrolyte showed very similar ORR performances for the ED-derived and the commercial catalysts.

Acknowledgements

The authors gratefully acknowledge the Department of Energy (DE-FC36-06G086041) and NSF (CTS-0456899) for funding this work.

References

[1] Z. Hou, B. Yi, H. Zhang, Electrochemical and Solid State Letters 6 (11) (2003) A232.
[2] I. Ohno, Materials Science and Engineering A 146 (1991) 33.
[3] A. Brenner, G.E. Riddell, Journal of Research of the National Bureau of Standards vol. 37 (31) (1946) 385.
[4] S.S. Djokic, in: B.E. Conway, R.E. White (Eds.), Modern Aspects of Electrochemistry, 35, Kluwer Academic/Plenum Publishers, Fort Saskatchewan, AB, Canada, 2002, p. 51.

[5] C. Kerr, D. Barker, F. Walsh, Transactions of the Institute of Metal Finishing 79 (1) (2001) 41.
[6] C.R.K. Rao, M. Pushpavanam, Materials Chemistry and Physics 68 (2001) 62.
[7] P. Steinmetz, S. Alperine, A. Friant-Costantini, P. Josso, Surface and Coatings Technology 43/44 (1990) 500.
[8] M. Paunovic, in: O.J. Murphy, S. Supramaniam, B.E. Conway (Eds.), Electrochemistry Transition, Plenum Publishers, New York, NY, 1992, p. 479.
[9] M.T. Schaal, A.Y. Metcalf, J.H.,W.J.P. Montoya, C.C. Stork, C.T. Williams, J.R. Monnier, Catalysis Today 123 (2007) 142.
[10] M.T. Schaal, A.C. Pickerell, C.T. Williams, J.R. Monnier, Journal of Catalysis 254 (2008) 131.
[11] K.D. Beard, M.T. Schaal, J.W. Van Zee, J.R. Monnier, Applied Catalysis B: Environmental 72 (2007) 262.
[12] A. Sepulveda-Escribano, F. Coloma, F. Rodriguez-Reinoso, Applied Catalysis A: General 173 (1998) 247.
[13] G. de la Puente, A. Centeno, A. Gil, P. Grange, Journal of Colloid and Interface Science 202 (1998) 155.
[14] J.L. Figueiredo, M.F.R. Pereira, M.M.A. Freitas, J.J.M. Orfao, Carbon 37 (1999) 1379.
[15] M.A. Fraga, E. Jordao, M.J. Mendes, M.M.A. Freitas, J.L. Faria, J.L. Figueiredo, Journal of Catalysis 209 (2002) 355.
[16] M.A. Fraga, M.J. Mendes, E. Jordao, Journal of Molecular Catalysis A: Chemical 179 (2002) 243.
[17] J.L. Gomez de la Fuente, S. Rojas, M.V. Martinez-Huerta, P. Terreros, M.A. Pena, J.L.G. Fierro, Carbon 44 (2006) 1919.
[18] M.F.R. Pereira, J.J.M. Orfao, J.L. Figueiredo, Applied Catalysis A: General 184 (1999) 153.
[19] M.C. Roman-Martinez, J.A. Diaz-Aunon, C. Salinas-Martines de Lecea, H. Alper, Journal of Molecular Catalysis A: Chemical 213 (2004) 177.
[20] A.R. Silva, M. Martins, M.M.A. Freitas, A. Valente, C. Freire, B. de Castro, J.L. Figueiredo, Microporous and Mesoporous Materials 55 (2002) 275.
[21] W. Xia, O.F.-K. Schlueter, C. Liang, M.W.E. van den Berg, M. Guraya, M. Muhler, Catalysis Today 102–103 (2005) 34.
[22] S.R. de Miguel, O.A. Scelza, M.C. Roman-Martinez, C. Salinas-Martines de Lecea, D. Cazorla-Amoros, A. Linares-Solano, Applied Catalysis A: General 170 (1998) 93.
[23] X. Hao, L. Quach, J. Korah, W.A. Spieker, J.R. Regalbuto, Journal of Molecular Catalysis A: Chemical 219 (2004) 97.
[24] J.T. Miller, M. Schreier, A.J. Kropf, J.R. Regalbuto, Journal of Catalysis 225 (2004) 203.
[25] M. Schreier, J.R. Regalbuto, Journal of Catalysis 225 (2004) 190.
[26] J.H. Yang, J.D. Henao, C. Costello, M.C. Kung, H.H. Kung, J.T. Miller, A.J. Kropf, J.-G. Kim, J.R. Regalbuto, M.T. Bore, H.N. Pham, A.K. Datye, J.D. Laeger, K. Kharas, Applied Catalysis A: General 291 (2005) 73.
[27] M. Pirjamali, Y. Kiros, Journal of Power Sources 109 (2002) 446.
[28] M. Gurrath, T. Kuretzky, H.P. Bloehm, L.B. Okhlopkova, A.S. Lisitsyn, V.A. Likholobov, Carbon 38 (2000) 1241.
[29] D.J. Suh, T.-J. Park, S.-K. Ihm, Carbon 31 (1993) 427.
[30] G.R. Heal, L.L. Mkayula, Carbon 26 (1988) 815.
[31] A.J. Bard, L.R. Faulkner, Electrochemical Methods: Fundamentals and Applications, second edition, John Wiley & Sons, New York, NY, 2001.
[32] J.G. Chen, C.A. Menning, M.B. Zellner, Surface Science Reports 63 (2008) 201.
[33] B. Hammer, J.K. Norskov, Advances in Catalysis 45 (2000) 71.
[34] M.P. Hyman, J.W. Medlin, Journal of Physical Chemistry C 111 (2007) 17052.
[35] K.D. Beard, Ph.D. Dissertation, University of South Carolina, 2008.
[36] S.R. Calvo, P.B. Balbuena, Surface Science 601 (2007) 165.
[37] K.D. Beard, S. Ma, J.W. Van Zee, J.R. Monnier, Journal of Physical Chemistry C (2008), in press.